

Alma Mater Studiorum Università di Bologna
Archivio istituzionale della ricerca

Relative knot probabilities in confined lattice polygons

This is the final peer-reviewed author's accepted manuscript (postprint) of the following publication:

Published Version:

Janse Van Rensburg, E.J., Orlandini, E., Tesi, M.C. (2025). Relative knot probabilities in confined lattice polygons. PHYSICAL REVIEW. E, 111(6), 065406-1-065406-12 [10.1103/PhysRevE.111.065406].

Availability:

This version is available at: <https://hdl.handle.net/11585/1028639> since: 2025-11-11

Published:

DOI: <http://doi.org/10.1103/PhysRevE.111.065406>

Terms of use:

Some rights reserved. The terms and conditions for the reuse of this version of the manuscript are specified in the publishing policy. For all terms of use and more information see the publisher's website.

This item was downloaded from IRIS Università di Bologna (<https://cris.unibo.it/>).
When citing, please refer to the published version.

(Article begins on next page)

Relative knot probabilities in confined lattice polygons

EJ Janse van Rensburg,¹ E Orlandini,² and MC Tesi³

¹*Department of Mathematics and Statistics,*

York University, Toronto, Ontario M3J 1P3,

Canada (Email: rensburg@yorku.ca)

²*Dipartimento di Fisica e Astronomia e Sezione INFN,*

Università di Padova, Via Marzolo 8,

I-35131 Padova, Italy (Email: orlandini@pd.infn.it)

³*Dipartimento di Matematica, Università di Bologna,*

Piazza di Porta San Donato 5, I-40126 Bologna,

Italy (Email: mariacarla.tesi@unibo.it)

(Dated: March 17, 2025)

Abstract

In this paper we examine the relative knotting probabilities in a lattice model of ring polymers confined in a cavity. The model is of a lattice knot of size n in the cubic lattice, confined to a cube of side-length L and with volume $V = (L+1)^3$ sites. We use Monte Carlo algorithms to approximately enumerate the number of conformations of lattice knots in the confining cube. If $p_{n,L}(K)$ is the number of conformations of a lattice polygon of length n and knot type K in a cube of volume L^3 , then the relative knotting probability of a lattice polygon to have knot type K , relative to the probability that the polygon is the unknot (the trivial knot, denoted by 0_1), is $\rho_{n,L}(K/0_1) = p_{n,L}(K)/p_{n,L}(0_1)$. We determine $\rho_{n,L}(K/0_1)$ for various knot types K up to six crossing knots. Our data show that these relative knotting probabilities are small so that the model is dominated by lattice polygons of knot type the unknot. Moreover, if the concentration of the monomers of the lattice knot is $\varphi = n/V$, then the relative knot probability increases with φ along a curve that flattens off as the Hamiltonian state is approached.

PACS numbers: 82.35.Lr, 82.35.Gh, 61.25.Hq

I. INTRODUCTION

The physical properties of polymers and biopolymers are affected by knotting and linking between polymeric strands [1–4]. In reference [5] a Flory theory for knotting ring polymers was proposed, and the probability of knotting in DNA were examined in references [6] and [7]. The effects of confinement on the knotting and entanglements of polymeric strands have been modelled using polygonal models [8, 9] and sampling randomly generated polygons in confining spaces (see, for example, the algorithms in references [10–14]). Knot probabilities have also been examined in randomly generated plane diagrams [15, 16], and other flat polygonal structures [17]. In these studies the consensus is that confining a polymer will increase the probability that it is knotted when undergoing ring closure [18, 19]. In the case of extremely strong confinement quantum-inspired coding was designed and used, for the first time, to characterise the entanglement of topologically unrestricted ring polymers at maximum packing density [20]. More results on the knotting probability in models of ring polymers are contained in references [3, 21–24].

There is also a comprehensive literature on the use of lattice models to examine the entanglement complexity of polymers. These are self-avoiding walk and lattice polygon models, and they model the self-avoidance of polymeric strands while also representing the topological complexity of polymers [3, 21, 23, 25] (also in the context of being squeezed into small volumes [26, 27]). A lattice polygon being stretched in one direction by a force, or adsorbed onto a hard wall, has reduced probability of knotting [17, 28–30], but when it has transitioned through the θ -point into a collapsed phase its knotting probability is increased [31]. It is also known that thermodynamic quantities are functions of knotting [26, 32, 33], and the osmotic pressure of compressed lattice knots is a function of knot type for finite size polygon models of ring polymers [34].

In this paper we use a lattice knot model of a ring polymer in a confined space to model the dependence of its knotting probability on its knot type. The lattice knot is compressed inside a confining cube, and also is a model of a biopolymer in a cavity or in a space between membranes. The compression and entanglement of single DNA molecules have been experimentally investigated [35, 36], and a lattice model of knotting in such confining conditions may give some insights into the results of these experiments even as the lattice may be an inadequate approximation. The aim here is to determine some quantitative results in

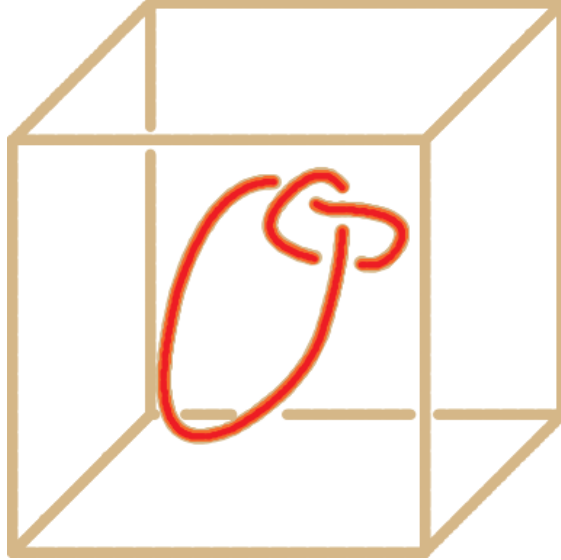


FIG. 1: A schematic drawing of a knot in a confining cube or box. The side length of the cube is L , and the knot has rotational, translational and conformational degrees of freedom. These contribute to the free energy of the system. Notice that the cube contains $(L+1)^3$ lattice sites so that its volume is $V = (L+1)^d$ sites.

the lattice to get qualitative insights into a complex physical situation, in particular insofar the relative incidence of knotting as a measure of entanglement of the polymeric molecules.

In Figure 1 a schematic diagram of the model is shown. The free energy of the model is quantified by the rotational, translational and conformational degrees of freedom of the knot inside the cube. In the cubic lattice the knot is a (self-avoiding) lattice polygon of knot type K , and its entropy is quantified by introducing the function $p_{n,L}(K)$ which is the number of conformations of the lattice knot if has length n and knot type K , and the confining cube has side length L and has $V = (L+1)^3$ lattice sites.

In section 2 we give a brief review of knot entropy and related issues. We will in particular be interested in the number of conformations of a lattice polygon of fixed knot type K . In section 3 we discuss the sampling of lattice knots using the GAS and GARM algorithms [24, 37, 38], and in section 4 we present and discuss the results of simulations. The paper is concluded in section 5 with a few final remarks.

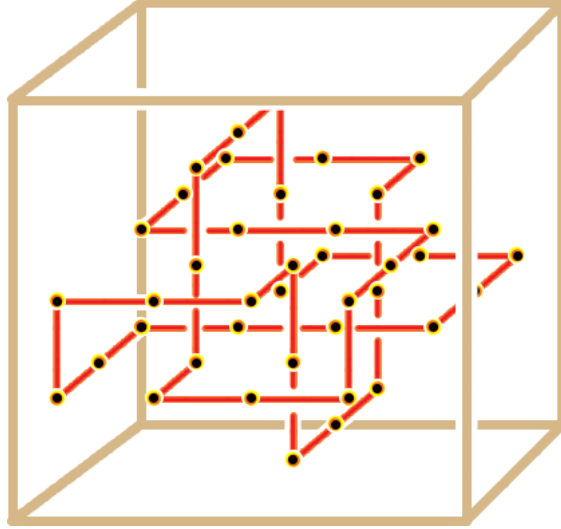


FIG. 2: A lattice knot in a cube in the cubic lattice. The side length of the cube is $L - 1$ (so that it contains $V = L^3$ sites).

II. LATTICE KNOTS

The number of cubic lattice *polygons* of length n is denoted p_n (these are unrooted and closed self-avoiding walks of length n steps in the cubic lattice counted up to equivalence under translations in the lattice). A *lattice knot* is a lattice polygon of a given (fixed) knot type K , and the number of lattice knots of length n and knot type K is denoted by $p_n(K)$.

A cubic lattice knot in a confining cube is shown in figure 2. The side-length of the cube is L in terms of lattice steps so that the cube contains $(L+1)^3$ lattice sites. The knot type of a lattice knot realised inside the cube (so that it is a cycle in the cube) is fixed, and so this is a model of a knotted ring polymer inside a confining volume, with fixed knot type. The lattice knot also has fixed length n (edges), and its distinct conformations (also due to translations and rotations inside the cube) is a model of the configurational entropy of a confined ring polymer. This model was explored in references [34, 39], where its free energy was modelled by Flory-Huggins theory, and the Flory Interaction Parameter of the model was estimated to be $\chi = 0.18(3)$ [39].

If $K = 0_1$ (the unknot), then $p_4(0_1) = 3$ in the cubic lattice, and $p_n(0_1) = 0$ if $n < 4$. This shows that the *minimal length* n_{0_1} of the unknot in the cubic lattice is 4 [2]. The minimal length of lattice knots of type K [40, 41] is denoted n_K , and for the trefoil knot 3_1 , $n_{3_1} = 24$ [42]. For the figure eight knot 4_1 , $n_{4_1} = 30$ and for the knot 5_1 , $n_{5_1} = 34$ [43]. Numerical

estimates of the minimal length of n_K of other knot types have also been determined, and for knots of low crossing number, those are exact with high probability (although unproven).

Since the cubic lattice is bipartite all lattice polygons have even lengths, so that $p_n(K) = 0$ if n is odd. By concatenating two lattice unknots (see reference [44]), it follows that, by Fekete's lemma, the limits

$$\lim_{n \rightarrow \infty} (p_n(0_1))^{1/n} = \mu_{0_1} < \mu = \lim_{n \rightarrow \infty} p_n^{1/n} \quad (1)$$

exist if these are taken through even values of n , where μ is the *growth constant* of self-avoiding cubic lattice polygons (or of the cubic lattice self-avoiding walk), and μ_{0_1} is the growth constant of lattice unknots. That $\mu_{0_1} < \mu$ was shown in reference [44].

Generally, the growth constant of cubic lattice knots of type K is defined by

$$\limsup_{n \rightarrow \infty} (p_n(K))^{1/n} = \mu_K. \quad (2)$$

It is known that $\mu_{0_1} \leq \mu_K < \mu$ (see, for example, [44, 45]), and it is believed that $\mu_K = \mu_{0_1}$ for all knot types K [23, 46]. There are strong numerical evidences that

$$p_n = C n^{\alpha-3} \mu^n (1 + o(1)) \quad (3)$$

$$p_n(K) = C_K n^{\alpha+N_K-3} \mu_K^n (1 + o(1)) \quad (4)$$

where C_K is an amplitude dependent on the lattice and the knot type K , $\alpha = 0.237(2)$ [47, 48] is the entropic exponent of lattice polygons and N_K is the number of prime knot components in the knot K [49].

Lattice knots in \mathbb{Z}^3 were sampled using both the GARM [38] and GAS [24, 37] algorithms, implemented with BFACF elementary moves [50–53]. Both these algorithms are approximate enumeration algorithms, returning estimates of $p_n(K)/p_m(K)$. Choosing m equal to the minimal length of the lattice knot of type K , and exactly counting $p_m(K)$, estimates of $p_n(K)$ for $n \geq m$ are obtained. Normally, one chooses $m = n_K$ and uses exact counts for $p_m(K)$ to determine estimates of $p_n(K)$ for $n > n_K$. For example, by equation (4) one expects $n p_n(0_1) \sim p_n(3_1)$. Generally, one expects that there is a value of ℓ such that

$$p_{n-\ell}(0_1) \simeq n^{-1} p_n(K), \quad \text{as } n \rightarrow \infty, \quad (5)$$

for a given prime knot type K . Plotting $\log [n p_{n-\ell}(0_1)/p_n(K)]$ as a function of $1/n$ for various values of ℓ shows that $\ell \approx 8$ when $K = 3_1$ is the trefoil knot [4, 24]. This shows that

tying a trefoil knot in a lattice polygon reduces the entropy of the polygon by reducing its length by about 8 steps. In addition, one notices that $p_n(0_1) > p_n(3_1)$ for small n , but these results show that $p_n(0_1) \approx p_n(3_1)$ if $n \approx 169600 \pm 5600$ and that $p_n(0_1) < p_n(3_1)$ for n larger than this, consistent with equation (4) [24].

The probability of knotting in polygons of length n sampled uniformly is

$$\mathbb{P}_n = 1 - p_n(0_1)/p_n = 1 - (C_{0_1}/C) (\mu_{0_1}/\mu)^n (1 + o(1)),$$

by equations (3) and (4). Since $\mu_{0_1} < \mu$ this shows that $\mathbb{P}_n \rightarrow 1$ as $n \rightarrow \infty$ (this is the Sumners-Whittington result in reference [44]). Numerical simulations in reference [54] shows that $\log(\mu/\mu_{0_1}) = (4.15 \pm 0.32) \times 10^{-6}$.

A. Lattice knots confined to cubes in the cubic lattice

Confined lattice knots have reduced state spaces dependent on the size of the confining cube. Decreasing the size of the confining cube reduces the conformational and, for short lattice knots, also the rotational and translational, degrees of freedom of the lattice knot. This models the reduction in entropy when a knotted ring polymer is compressed in a cavity.

Denote the number of placements of lattice polygons (as opposed to lattice knots) of length n in a cube of side-length L (this is an L -cube) by $p_{n,L}$. The number of lattice knots of length n and knot type K , confined to an L -cube of sidelength L containing $(L+1)^3$ lattice sites (as illustrated in figure 2), is denoted by $p_{n,L}(K)$. For example, for the unknot with $n = 4$ and $L = 1$, $p_{4,1}(0_1) = 6$ (these are minimal length unknots of length b in a cube of sidelength $L = 1$). Notice that, in general, both conformational and translational degrees of freedom contribute to the counts $p_{n,L}(K)$. There are few exact results available for $p_{n,L}(K)$, but clearly,

$$p_{n,L}(K) = 0, \quad \text{if } n < n_K \text{ or } n > L^3. \quad (6)$$

For minimal length lattice knots and various knot types, $p_{n,L}(K)$ can be evaluated by exhaustively counting their number of placements in L -cubes. These are shown in table I (these counts are, strictly speaking, lower bounds, but should be exact in most cases, as they were checked exhaustively by repeated computer searches).

The free energy of lattice knots of type K in an L -cube was examined numerically in references [34, 39]. The lattice free energy density of compressed lattice knots can be defined

TABLE I: Table I: Number of lattice knots $p_{n,L}(K)$ of minimal length n_K in an L -box

L -Box	0_1	3_1^+	4_1	5_1^+	5_2^+	6_1^+	6_2^+	6_3	$3_1^+ \# 3_1^+$	$3_1^+ \# 3_1^-$
1	6	0	0	0	0	0	0	0	0	0
2	36	0	0	0	0	0	0	0	0	0
3	108	2084	864	0	0	0	0	0	0	108
4	240	15052	14048	9840	123312	6144	14568	4032	1332	33192
5	450	48876	73440	52416	740232	37512	134928	32496	61452	634752
6	756	113540	188928	147504	2186976	112329	459480	106272	222456	2201904
7	1176	219028	386400	315120	4808280	249000	1086720	246672	530280	5166360
8	1728	375324	687744	575280	8948880	465984	2115144	475008	1030860	9959832
9	2430	592412	1114848	948000	14953512	781704	3643248	812592	1770132	17014032
10	3300	880276	1689600	1453296	23166912	1214592	5769528	1280736	2794032	26760672
11	4356	1248900	2433888	2111184	33933816	1783080	8592480	1900752	4148496	39631464
12	5616	1708268	3369600	2941680	47598960	2505600	12210600	2693952	5879460	56058120
13	7098	2268364	4518624	3964800	64507080	3400584	16722384	3681648	8032868	76472352
14	8820	2939172	5902848	5200560	85002912	4486464	22226328	4885152	10654632	101305872
15	10800	3730676	7544160	6668976	109431192	5781672	28820928	6325776	13790712	130990392
n_K	4	24	30	34	36	40	40	40	40	40

by

$$F_V(\varphi) = -\frac{1}{V} \log p_{n,L}(K) \quad (7)$$

where $V = (L+1)^3$ is the number of sites of the confining L -cube, and $\varphi = n/V$ is the concentration of monomers. The free energy *per unit length* is similarly given by

$$f_K(\varphi) = -\frac{1}{n} \log p_{n,L}(K). \quad (8)$$

In figure 3 estimates of $f_K(\varphi)$ of lattice unknots ($K = 0_1$) in L -cubes for $L \in \{6, 8, 10, 12, 14\}$ are plotted as a function of the concentration φ . In references [34, 39] these free energies, and the lattice osmotic pressure were examined using a Flory-Huggins approximation [55–57]. In these models the appropriate Flory-Huggins approximation is a mean-field model and a

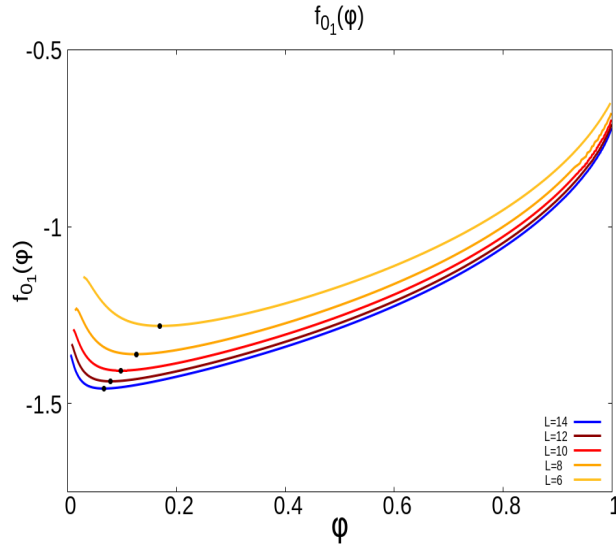


FIG. 3: Free energy curves of lattice unknots (see equation (8)) for $L \in \{6, 8, 10, 12, 14\}$. The curves appear to converge to a limiting curve with increasing L and have minima at a critical concentration φ_c (dependent on L). The minima are marked by a bullet on each curve.

function of the concentration φ given by

$$f_{fh}(\varphi) = (1-\varphi) \log(1-\varphi) + (\varphi/n) \log \varphi - \chi \varphi^2 + A\varphi. \quad (9)$$

Here, χ is the Flory Interaction Parameter [55–57], n is the degree of polymerization (length of the polymer) and the term $A\varphi$ accounts for a (bulk) entropic contribution to the free energy of mixing due to conformational degrees of freedom of the lattice polymer. Taking first $n \rightarrow \infty$, and then $\varphi \rightarrow 0^+$, show that $(f_{fh}(\varphi))/\varphi \rightarrow A-1$. Thus $A = 1 - \log \mu$, where $\log \mu$ is the connective constant of the lattice (see reference [34] for more details). Figure 4 is a schematic diagram of $f_{fh}(\varphi)$.

The free energy curves in figure 3 are convex functions of φ passing through minima at concentrations φ^* . In figure 3 these minima are marked by bullets, and they decrease with increasing L (size of the containing L -cube).

In the Flory-Huggins approximation a critical concentration φ_c (see figure 4) is determined by the thermodynamic stability criteria $\frac{\partial^2}{\partial \varphi^2} f_{fh}(\varphi) = 0$ and $\frac{\partial^3}{\partial \varphi^3} f_{fh}(\varphi) = 0$, taken at fixed n (and temperature) (see reference [58] for a good review). These give the approximate location of a critical concentration $\varphi_c = 1/(1+\sqrt{n_c})$ where n_c is the length of the lattice polymer

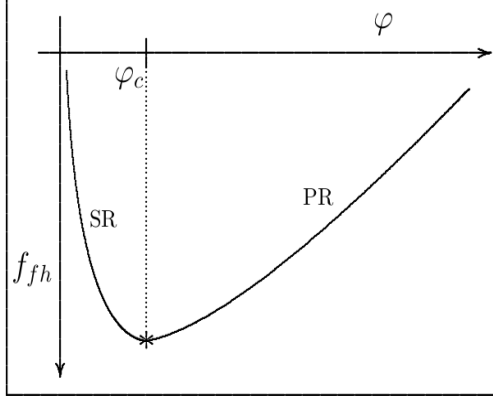


FIG. 4: A schematic representation of the Flory-Huggins free energy. The convex curve has a minimum at φ_c , separating the model into two regimes, namely a solvent-rich (SR) phase at low concentrations $\varphi < \varphi_c$, and a polymer-rich (PR) phase at high concentrations $\varphi > \varphi_c$. The regimes are separated at the critical concentration φ_c . In the vicinity of φ_c the system is in θ -conditions.

at the critical concentration. Since $\varphi_c = n_c/(L+1)^3$ this expression is a self-consistent equation for the critical concentration φ_c . For large L this gives $\varphi_c \approx 1/(1 + \sqrt{\varphi_c(L+1)^3})$, and assuming that $1 \ll \sqrt{(L+1)^3} \ll (L+1)^3$, one approximates $\varphi_c \approx 1/\sqrt{\varphi_c(L+1)^3}$ or $\varphi_c^{3/2} \approx 1/\sqrt{(L+1)^3}$. Squaring both sides and taking the cube root gives the (Flory-Huggins) critical concentration as a function of L :

$$\varphi_c \approx 1/(L+1), \quad (10)$$

where $(L+1)^3$ is the volume (total number of lattice sites) in the containing L -cube. For example, if $L = 6$, then $\varphi_c \approx 1/7 = 0.1428\dots$. While not equal to, this approximates the minimum in the free energy curve for $L = 6$ in figure 3 well (for $L = 6$ the minimum is located at $\varphi^* \approx 0.169$). Similar observations are valid for the other values of L , for example, if $L = 12$ then $\varphi_c \approx 1/13 = 0.0769\dots$ while $\varphi^* \approx 0.0792$ and if $L = 14$ then $\varphi_c \approx 1/15 = 0.0667\dots$ while $\varphi^* \approx 0.067$. Notice that $\varphi_c \approx 1/(L+1)$ also corresponds to $n_c \approx (L+1)^2$. Following the analysis in reference [58] the critical concentration divides the free energy curves into two regimes – for concentrations $\varphi < \varphi_c$ the model is in a *solvent-rich* regime where the lattice polymer has self-avoiding walk exponents, and for $\varphi > \varphi_c$ the model is in a *polymer-rich* regime where the lattice polymer is in a collapsed state, compressed into this phase by being confined in the containing cube. See for example figure 6 in reference [58].

In this paper our focus is on the entanglements of the polymer as a function of the concentration φ , namely as it increases from the solvent-rich regime to the polymer-rich regime when φ passes through its critical value at φ_c . Simulations in reference [59] suggest that the degree of entanglement complexity of two lattice knots increases as the model is taken through the θ -point into the collapse phase. This result is consistent with numerous earlier studies [9, 13, 19, 31]. Consistent with these studies, one expects an increase in the self-entanglement of the lattice polymer with φ , and we examine this in our model by estimating knot probability ratios.

B. Knotting probabilities in confined lattice knots

The probability that a randomly placed lattice polygon of length n in an L -cube is a knot of type K is defined by

$$\mathbb{P}_{n,L}(K) = \frac{p_{n,L}(K)}{p_{n,L}}. \quad (11)$$

In the event that $L \gg n$, $p_{n,L} \simeq L^3 p_n$ and $p_{n,L}(K) \simeq L^3 p_n(K)$. This shows that

$$\lim_{L \rightarrow \infty} \mathbb{P}_{n,L}(K) = \frac{p_n(K)}{p_n}. \quad (12)$$

Since $\mu_K < \mu$ [44] it follows by equations (3) and (4) that taking $n \rightarrow \infty$,

$$\lim_{n \rightarrow \infty} \lim_{L \rightarrow \infty} \mathbb{P}_{n,L}(K) = 0. \quad (13)$$

That is, in the limit of very large cubes the probability that a lattice knot has a specified knot type K approaches zero. This is valid for any knot type K , including the unknot 0_1 . Interchanging the order of the limits above, putting $N = 2\lfloor L^3/2 \rfloor$ one arrives at

$$\lim_{L \rightarrow \infty} \lim_{n \rightarrow N} \mathbb{P}_{n,L}(K) = \pi_K, \quad (14)$$

which may be interpreted as the limiting probability that a polygon of maximum length N in a lattice cube has knot type K . In the case that L is taken to infinity through even numbers, this is the limiting knotting probability of Hamiltonian cycles of a cube as the size of the cube expands to infinity.

In general, for finite and fixed L , $\mathbb{P}_{n,L}(K)$ is a function of L and of $\varphi = n/V$, (the *concentration* or *density of monomers* in a cube of sidelength L). We shall see that numerical estimates of $\mathbb{P}_{n,L}(K)$ are not directly accessible, since algorithms sampling lattice knots in

confined geometries are either not efficient as the concentration of occupied lattice sites becomes high (one may, for example, use the pivot algorithm for lattice polygons [60, 61], but this algorithm has a very low success rate of proposed elementary moves when the concentration of occupied sites is high). Other algorithms are also inefficient or are only useful to sample polygons of fixed knot type in confining spaces (see references [34, 39]), and cannot directly be used to determine knotting probabilities.

Since the GARM and GAS algorithms can be used to determine approximate counts of states when sampling lattice clusters, it is possible to estimate ratios of knotting probabilities. That is, estimates of

$$\rho_{n,L}(K_1/K_2) = \frac{p_{n,L}(K_1)}{p_{n,L}(K_2)} = \frac{\mathbb{P}_{n,L}(K_1)}{\mathbb{P}_{n,L}(K_2)} \quad (15)$$

can be obtained by taking ratios of the estimates of $p_{n,L}(K)$ for various knot types K using the GARM or GAS algorithms. In the case that the lattice knots fill the L -cube, define

$$R_L(K_1/K_2) = \lim_{n \nearrow V} \rho_{n,L}(K_1/K_2) = \lim_{n \nearrow V} \frac{\mathbb{P}_{n,L}(K_1)}{\mathbb{P}_{n,L}(K_2)}. \quad (16)$$

This is the (limiting) ratio of probabilities of knot types K_1 and K_2 as the polygon approaches a Hamiltonian cycle inside the cube. The ratio $\rho_{n,L}(K_1/K_2)$ is generally a function of the concentration of monomers φ , and its size indicates the relative incidence of knot type K_1 (rather than knot type K_2) if states are sampled uniformly. That is, if $\rho_{n,L}(K_1/K_2) < 1$ then one expects the knot type K_2 to be realised in lattice knots inside the confining cube more abundantly than knot type K_1 . This quantity will be examined for various knot types in the next sections of this paper. In particular, the case that $K_2 = 0_1$ gives the ratio of a knot type K_1 compared to the unknot. If $R_L(K_1/0_1) < 1$, then the knot type K_1 is suppressed compared to the unknot, and this is what the data will show when L is finite.

III. SAMPLING LATTICE KNOTS CONFINED TO CUBES IN THE CUBIC LATTICE

The GAS [37] and GARM [38] algorithms were implemented using BFACF elementary moves [50, 51] to sample lattice knots inside an L -cube of fixed size. Normalising the results using the data in table I, approximate counts of the number of distinct lattice knots of length n (with $n_K \leq n \leq L^3$) can be obtained. The implementation of these algorithms was along

4 parallel threads (and in some cases, 6 parallel threads) using a parallel implementation similar to that of parallel PERM [62]. Our results were obtained using the GAS implementation and additional short simulations were done using the GARM algorithm to verify our results.

Each GAS simulation was done in B blocks, each block consisting of T parallel threads, and each thread with S iterations. For example, in a 12-cube with 2197 sites, lattice knots of length $n \leq 2196$ were sampled using $B = 120$ blocks, each block having $T = 4$ parallel threads and each call to a thread having $S = 20,000,000$ BFACF iterations (for a total of $BST = 9,600,000,000$ BFACF elementary moves collecting data on lattice knots for lengths between $n_K = 4$ and maximum length 2196 in the case that $K = 0_1$). The number of blocks increased from 60 for $L = 6$ to 150 for $L = 14$, and the lengths of threads from 20,000,000 for $L = 6$ to 30,000,000 for $L = 14$.

Since the data collected in each block becomes independent from other blocks, rough estimates of the error bar on the results can be obtained. While the error is relatively small, it increases in size with the length of the lattice knot but shows that the order of magnitude of the approximate counts is accurate. For example, if $L = 12$ and the lattice unknot is sampled, then for $n = 10$ one gets $p_{10,12}(0_1) = (8.55 \pm 0.28) \times 10^5$ and $p_{1000,12}(0_1) = (3.04 \pm 1.54) \times 10^{563}$. While the error bar in the last estimate appears large, it is the case that $\log p_{1000,12}(0_1) = 1297.5 \pm 1.2$, with an acceptable error bar.

The algorithms were implemented and data were collected through several months, resulting in data being available for L -cubes of sizes $L \in \{6, 8, 10, 12\}$ and also $L = 14$ for the unknot and trefoil knot types. Lattice knots sampled in 12-cubes had lengths up to $13^3 - 1 = 2196$, but convergence was generally good only for concentrations $\varphi \lesssim 0.93$. This was similarly the case for sampling in 14-cubes (where lattice knots of length up to $15^3 - 1 = 3374$ were sampled, but convergence was achieved when $\varphi \lesssim 0.90$). Convergence for smaller values of L was generally better, resulting in shorter simulations, although sampling for high values of φ remained challenging. Generally, for concentrations $\varphi \gtrsim 0.93$ the ratios $\rho_{n,L}(K_1/K_2)$ were noisy and no conclusions could be drawn.

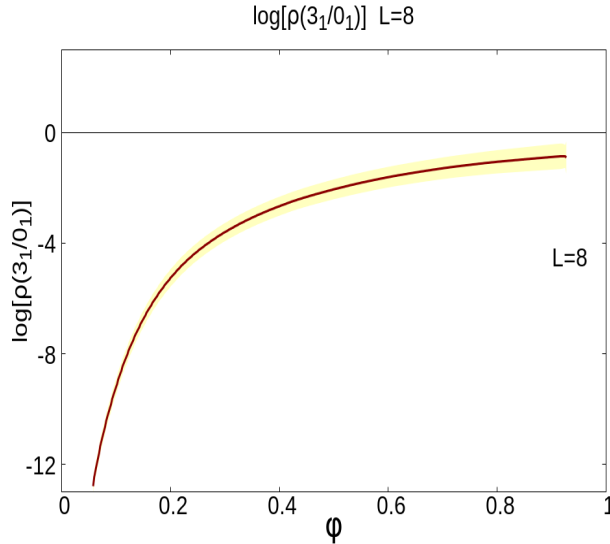


FIG. 5: The knot probability ratio $\rho_{n,L}(3_1^+/0_1)$ of trefoils to unknots for $L = 8$ (see equation (15)) plotted against the concentration φ . Notice the logarithmic scale and that trefoils are rare compared to unknots in this model of compressed lattice knots. With increasing concentration the ratio increases monotonically, but remains small. The confidence interval is shown by the shaded area around the curve and was determined by combining the standard deviations calculated for the raw data and then combined via the ratio in equation (15).

A. The relative incidence of unknots and trefoils

Figure 5 is a plot of $\rho_{n,L}(3_1^+/0_1)$ as a function of φ for $L = 8$. The knotting probability of trefoils (3_1^+), relative to the unknot (0_1), increases monotonically with the concentration φ and eventually levels off for sufficiently large values of φ . The shaded band around the curve is a standard deviation confidence interval. At $\varphi \approx 0.5$ the relative knotting probability is roughly 0.10 indicating that the number of trefoil lattice knots is approximately only 10% of the corresponding unknots (0_1). In other words, compared to unknotted lattice knots, trefoils are relatively rare. Similar data are shown for $L = 12$ in figure 6. In this case the relative incidence of trefoils compared to unknots is larger compared to unknots, increasing from low values (less than 0.10 for $\varphi < 0.3$) to approach 1.0 when $\varphi > 0.8$. The uncertainty envelope in this figure is also wider giving a large uncertainty envelope when φ exceeds approximately 0.5. In both figures 5 and 6 the curves level off as the concentration

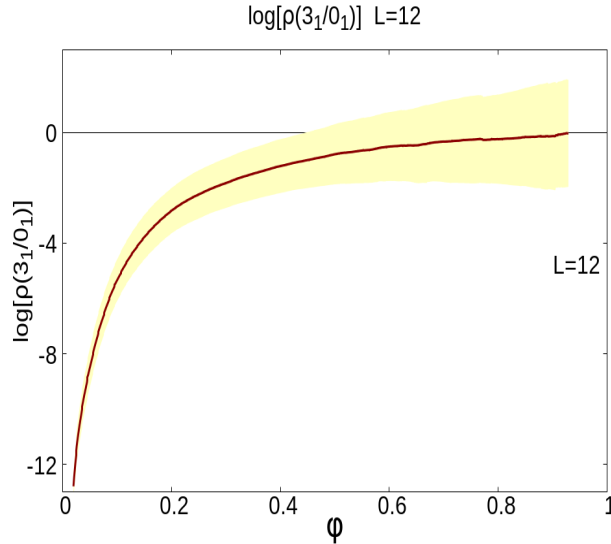


FIG. 6: The knot probability ratio $\rho_{n,L}(3_1^+/0_1)$ of trefoils to unknots for $L = 12$ (see equation (15)) plotted against the concentration φ . The scaling along the axes is the same as in figure 5, and with increasing concentration, the ratio increases monotonically, although it is still small in this larger confining cube at low concentrations but increases to 1 as the concentration increases beyond 0.8. The confidence interval is again shown by the shaded area around the curve.

approaches 1, indicating that the number of knotted polygons (of type trefoil) comes closer to the number of unknotted polygons as the Hamiltonian limit is approached. However, these data also show that the unknot is a more popular knot type compared to the trefoil over the entire range of concentration, in particular for small values of L .

In figure 7 the φ dependence of the trefoil-unknot ratio $\rho_{n,L}(3_1^+/0_1)$ is reported for several confining L -cubes with $L \in \{6, 8, 10, 12, 14\}$. For fixed concentration φ the ratios increase systematically with L , and there is also a levelling off at larger values of L . The curves appear to approach a limiting curve (especially if the increase in volume of the L -cube proportional to $O(L^3)$ is taken into account). However, even if the data are suggestive, the numerical simulations at larger values of $L \geq 12$ pose significant challenges. If these curves approach a limiting value less than 1 (that is, if $\limsup_{L \rightarrow \infty} \rho_{n,L}(3_1^+/0_1) < 1$ when the limsup is taken at constant concentration), then trefoils remain suppressed compared to unknots, even in the continuum limit. However, the data appear to show that the curves accumulate, with increasing L , on the horizontal axis, so that $\rho_{n,L}(3_1^+/0_1) \rightarrow 1$ as $L \rightarrow \infty$ for Hamiltonian

polygons.

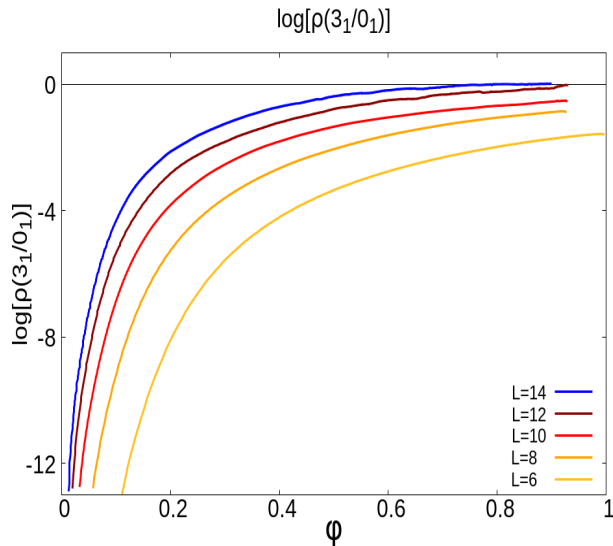


FIG. 7: The knot probability ratio $\rho_{n,L}(3_1^+/0_1)$ of trefoils to unknots for $L \in \{6, 8, 10, 12, 14\}$ plotted against the concentration φ . The scaling along the axes is the same as in figure 5. With increasing L the ratio increases but also suggests that the ratio may be approaching a limiting curve less than 1 but approaching 1 as the concentration approaches 1.

Note that the probability ratios in figure 7 increase with the concentration φ , and sharply so as φ transitions from below $\varphi_c \approx 1/(L+1)$ (the solvent-rich regime) to above φ_c in the polymer-rich or collapsed regime. This is consistent with other studies on lattice knot probabilities. Lattice knots are generally smaller the more complex the knot type is [63]. Therefore, more complex knot types are more likely to occur when a polygon is compressed [19, 32], or when the lattice polygon is in a more concentrated (collapsed) regime [8, 9, 13, 31].

Additionally, the curves in figure 7 flatten out as the concentration increases above 0.7. This shows that the incidence of knots of type 3_1^+ becomes stable when compared to unknots, suggesting that there is a stable ratio of lattice knots of unknot and trefoil types for fixed φ that increases approaching the Hamiltonian state. In this case one would be interested in the limiting ratio

$$R(3_1^+/0_1) = \lim_{L \rightarrow \infty} \lim_{\varphi \rightarrow 1^-} \rho_{n,L}(3_1^+/0_1) \leq 1. \quad (17)$$

Interesting questions to be addressed are whether $R(3_1^+/0_1) < 1$ and if its value is universal

(that is, independent of the model, and so an intrinsic property of the knot types for dense curves).

The curves in figure 7 appear to start converging with increasing φ , but the accessible data point is only suggestive. Only simulations at larger values of L , and successful collection of data for φ close to 1, would settle these questions, but are also outside the realm of what is possible using our current algorithms and computer hardware.

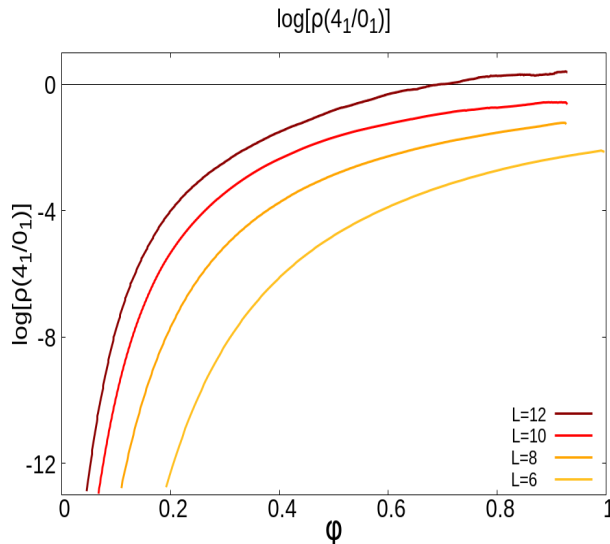


FIG. 8: The relative knot probability ratio $\rho_{n,L}(4_1/0_1)$ of figure eight knots (4_1) to unknots for $L \in \{6, 8, 10, 12\}$ plotted against the concentration φ . The scaling along the axes is the same as in figure 5.

B. The relative incidence of other prime knots

The knot probability ratios $\rho_{n,L}(K/0_1)$ of other prime knots of type K with respect to the unknots were also estimated by collecting data on the figure eight knot (4_1), and five and six crossing prime knots in the standard knot tables (namely knot types 5_1 and 5_2 , and the six crossing knots 6_1 , 6_2 and 6_3 and the compound six crossing knots $3_1^+ \# 3_1^+$ and $3_1^- \# 3_1^+$). In these cases lattice knots were sampled in confining cubes of side-lengths $L \in \{6, 8, 10, 12\}$, and again scaled using the data in table I.

In figure 8 the relative knot probability ratios $\rho_{n,L}(4_1/0_1)$ of the figure eight ($K = 4_1$) are shown. Comparing the curves in figure 8 to those reported in figure 7 for knot type 3_1^+ shows

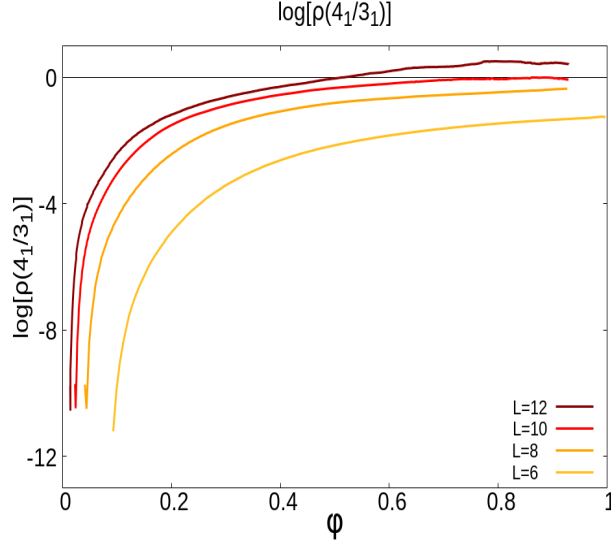


FIG. 9: The relative knot probability ratio $\rho_{n,L}(4_1/3_1^+)$ of figure eight knots (4_1) to the trefoil knot (3_1^+) for $L \in \{6, 8, 10, 12\}$ plotted against the concentration φ . The scaling along the axes is the same as in figure 5.

that the ratios for 4_1 are lower than the corresponding ratios for 3_1^+ , with the exception of the curve for $L = 12$ at high concentration (examination of our data shows that this curve is more noisy at large concentration). This indicates that, generally, 4_1 lattice knots are less likely to occur than the corresponding lattice knots of knot type 3_1^+ . Note that the curves in figure 8 do have the same general behaviour as seen for 3_1^+ in figure 7, but they do increase more sharply as the concentration φ increases from the solvent-rich regime $\varphi < \varphi_c$ to the polymer-rich regime $\varphi > \varphi_c$.

The relation between 3_1^+ and 4_1 may be better explored by plotting the φ dependence of the knot probability ratio $\rho_{n,L}(4_1/3_1^+)$, see figure 9. In these cases the data are consistent with $\rho_{n,L}(4_1/3_1^+) < 1$ generally (except for $L = 12$ at high concentration where the curve appears more noisy), indicating that the probability of 4_1 is generally less than that of 3_1^+ . As L increases, the ratio $\rho_{n,L}(4_1/3_1^+)$ appears to approach 1 (the confidence interval, as suggested in figures 5 and 6 widens with increasing concentration, and the horizontal axis is well within it at high concentration). This suggests that the incidence of knot types 4_1 and 3_1^+ may become similar for large L , at least as the concentration approaches 1. However, for low concentrations it is not evident that $\rho_{n,L}(4_1/3_1^+)$ is approaching 1 as L increases, but this cannot be ruled out.

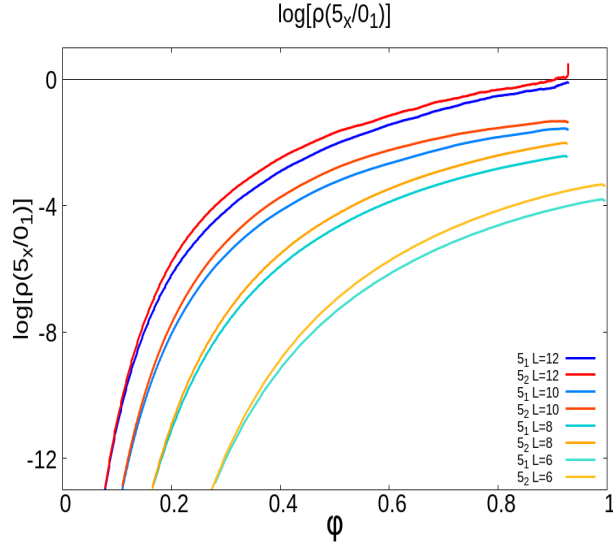


FIG. 10: The relative knot probability ratio $\rho_{n,L}(5_x/0_1)$ of figure eight knots (5_x) to unknots for $L \in \{6, 8, 10, 12\}$ plotted against the concentration φ . The scaling along the axes is the same as in figure 5.

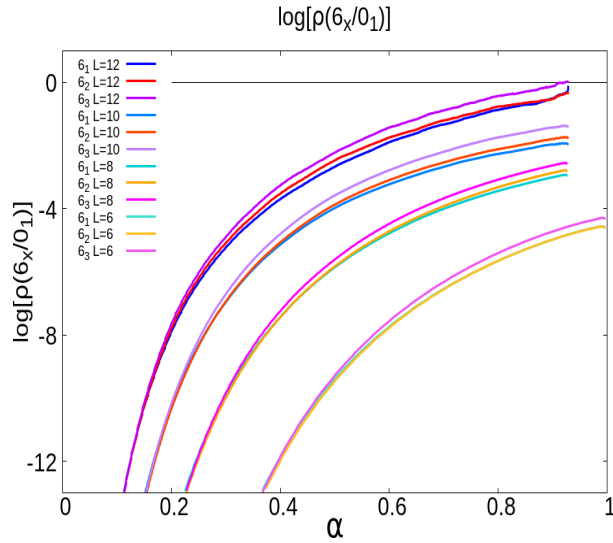


FIG. 11: The relative knot probability ratio $\rho_{n,L}(6_x/0_1)$ of figure eight knots (6_x) to unknots for $L \in \{6, 8, 10, 12\}$ plotted against the concentration φ . The scaling along the axes is the same as in figure 5.

In figure 10 the relative probabilities of the five crossing knots 5_1 and 5_2 with respect to the unknot 0_1 are plotted against concentration for different values of L . One notices that the

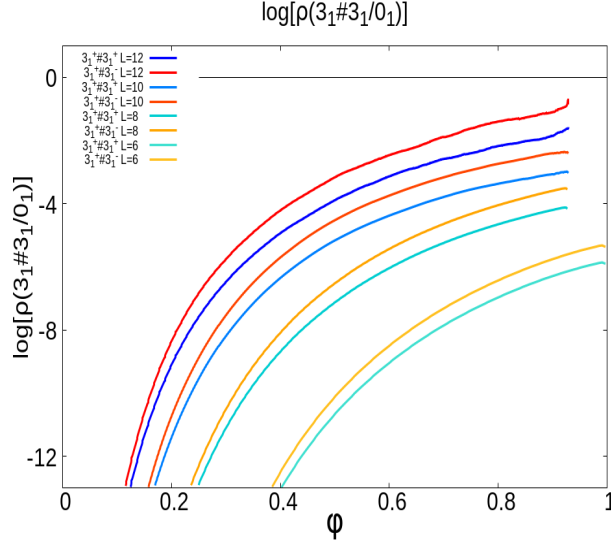


FIG. 12: The relative knot probability ratio $\rho_{n,L}(3_1\#3_1/0_1)$ for two compounded trefoil knots of types $3_1^+\#3_1^+$ and $3_1^+\#3_1^-$ to unknots for $L \in \{6, 8, 10, 12\}$ plotted against the concentration φ . The scaling along the axes is the same as in figure 5.

incidence of five-crossings knots is suppressed compared to the trefoil or figure eight knots. Moreover, knot type 5_2 is more likely to occur, compared to 5_1 . Similar plots are reported in figure 11 for the six crossing knot types 6_1 , 6_2 and 6_3 . Of these three knot types, 6_3 is the most likely, followed by 6_2 and 6_1 . Finally, the relative probabilities of the compound knots $3_1^+\#3_1^-$ and $3_1^+\#3_1^+$ are shown in figure 12, and $3_1^+\#3_1^-$ has a higher probability of occurring.

The relative knot probability of knot types for $L = 12$ are ranked in table II by listing $\log p_{n,L}(K)$ in decreasing size for $n = 500$. The data for $n = 1000$ and $n = 2000$ are also listed for comparison, and are generally consistent with the ranking at $n = 500$, except in a few cases. For example, although not separated by the error bars, the knot type 4_1 appears to outrank the unknot and 3_1^+ when $n = 2000$, but a large confidence interval shows that this is likely due to uncertainties in the data. However, the general trend in the table is that increasing the crossing number suppresses the number of conformations of a lattice knot, and so reducing its probability of being sampled if lattice knots are sampled uniformly. This is in particular the case for small values of L . Generally, the unknot outranked all the non-trivial knot types, and by a wide margin at low concentration. It is not clear that this observation will persist with increasing L and concentration, as shown in table II and in the graphs of $\rho_{n,L}(K/0_1)$ in figures 7 to 10.

TABLE II: Estimates of $\log p_{n,L}(K)$ in an L -cube
with $L = 12$ in descending order

Knot type	$n = 500$	$n = 1000$	$n = 2000$
0_1	699.69(45)	1297.48(52)	1816.77(93)
3_1^+	697.22(41)	1296.51(50)	1816.71(99)
4_1	696.23(43)	1296.36(52)	1817.98(160)
5_2^+	694.64(45)	1295.97(54)	1816.83(76)
5_1^+	694.19(37)	1295.06(46)	1816.59(81)
6_3	693.02(49)	1294.81(62)	1816.75(99)
6_2^+	692.86(47)	1294.56(52)	1816.36(81)
6_1^+	692.74(57)	1294.38(61)	1816.13(79)
$3_1^+ \# 3_1^-$	692.24(45)	1291.56(55)	1815.77(75)
$3_1^+ \# 3_1^+$	691.49(65)	1293.15(72)	1815.02(91)

IV. CONCLUSIONS

Our numerical results show that the unknot is the most popular knot type when lattice knots are compressed in an L -cube, for values of L up to $L = 14$. This is in particular the case for low to moderately high concentrations. In figure 7 the curves of knot probabilities of the trefoil relative to the unknot suggest that the trefoil will remain rare compared to unknots for small values of L . This is less clear with increasing L ; while the rate of change in the curves of $\rho_{n,L}(3_1^+/0_1)$ decreases with increasing L , these curves may reach a limiting curve at zero. Additionally, as the concentration φ increases the relative knotting probability, while still increasing, flattens out to a limiting value less than zero as the Hamiltonian state is reached for smaller values of L . These observations also apply to the other knot types examined. However, we expect that unknots will become rare as L increases, compared to all non-trivial knot types, but the possibility that the unknot is dominant compared to any other fixed non-trivial knot types appear likely for low concentration. That is, in the limit that L is large, and polygons are sampled uniformly from a confining cube, one expects

non-trivial knot types to be far more likely than unknots. However, unknots may still be the single most likely knot type, consistent with our numerical results.

Additionally, the likelihood of knotted conformations in an L -cube increases with φ as the model passes through the critical concentration φ_c separating the solvent-rich and polymer-rich regimes. Thus, an increase in knotting (and thus entanglement) is expected as the concentration increases towards the limit of Hamiltonian cycles of the cube. In other words, in the dense phase entanglements, as measured by the knotting of the lattice polygons, is strongly enhanced,

TABLE III: Limiting probability ratio $R_L(K_1/K_2)$
(equation (16))

L	$3_1^+/0_1$	$4_1/0_1$	$4_1/3_1^+$	$5_1^+/0_1$	$5_2^+/0_1$
6	-1.538(60)	-2.030(9)	-1.507(54)	-3.689(13)	-3.197(14)
8	-0.832(23)	-1.059(22)	-0.404(21)	-2.185(29)	-1.765(39)
10	-0.572(36)	-0.377(36)	-0.137(31)	-1.391(42)	-1.049(45)
12	-0.391(34)	0.291(42)	-0.051(29)	-0.363(48)	-0.070(51)
14	-0.301(24)				

TABLE IV: Limiting probability ratio $R_L(K_1/0_1)$
(equation (16)) for 6 crossing knots

L	$6_1^+/0_1$	$6_2^+/0_1$	$6_3/0_1$	$3_1^+\#3_1^+/0_1$	$3_1^+\#3_1^-/0_1$
6	-4.424(27)	-4.416(19)	-4.152(23)	-5.736(18)	-5.200(22)
8	-2.602(47)	-2.460(47)	-2.216(52)	-3.796(50)	-3.190(46)
10	-1.655(54)	-1.481(55)	-1.113(57)	-2.727(63)	-2.100(54)
12	-0.431(59)	-0.330(58)	0.009(63)	-1.670(66)	-0.983(59)

In table III we plot the logarithms of the limiting probability ratios $R_L(K_1/K_2)$ as defined in equation (16). These ratios correspond to the extrapolation of $\rho_L(K_1/K_2)$ to $\varphi = 1$ (in other words, to a space filling (Hamiltonian) curve in the confining cube). For example, if

the curve in figure 5 is extrapolated then $\log R_8(3_1^+/0_1) = -0.832 \pm 0.023$. The extrapolation was done assuming the model

$$\begin{aligned} \log \rho_L(K_1/K_2) = \log R_L(K_1/K_2) & \quad (18) \\ & + b(1/\varphi - 1) + c(1/\varphi^2 - 1) \end{aligned}$$

and performing a weighted least squares fit and discarding data at small values of φ (typically, we fitted against data for $\varphi > 0.1$).

In table III there is a systematic decrease in the size of $\log R_L(K_1/K_2)$ down the columns, showing that non-trivial knot types generally become more competitive with the unknot as L increases. However, the dominance of the unknot remains substantial for smaller values of L , even as the limiting ratio $\log R_L(4_1/3_1^+)$ approaches zero with increasing L (this indicates that the probability of knot type 4_1 may become comparable to that of the trefoil knot type 3_1^+ as the size of the confining cube increases).

The variation along rows in table III are more uneven, indicating that some knot types are more likely to occur than others. For example, comparing the knot types 5_1 and 5_2 shows that 5_2 is more likely than 5_1 in the limit that $\varphi \nearrow 1$. Similar observations are valid for the knot types 3_1^+ and 4_1 . In table IV all the six crossing prime and compound knot types are listed. An examination of the results show that generally, except for $L = 6$, amongst the six crossings knots the knot type 6_3 the most likely. The six crossing compound knot types $3_1^\pm \# 3_1^\pm$ are suppressed compared to the prime six crossing knots, and with the knot type $3_1^+ \# 3_1^-$ more likely than $3_1^+ \# 3_1^+$ (or $3_1^- \# 3_1^-$).

Acknowledgements

EJJvR acknowledges financial support from NSERC (Canada) in the form of Discovery Grant RGPIN-2019-06303. MCT acknowledges membership of GNAMPA (Gruppo Nazionale per l'Analisi Matematica, la Probabilità e le loro Applicazioni) of INdAM (Istituto Nazionale di Alta Matematica), Italy.

-
- [1] M Delbrück. Knotting problems in biology. *Proc Symp Appl Math*, 14:55–63, 1962.
 - [2] P-G de Gennes. Tight knots. *Macromol*, 17:703–704, 1984.

- [3] K Koniaris and M Muthukumar. Knottedness in ring polymers. *Phys Rev Lett*, 66:2211–2214, 1991.
- [4] M Baiesi and E Orlandini. Universal properties of knotted polymer rings. *Phys Rev E*, 86:031805, 2012.
- [5] AY Grosberg, A Feigel, and Y Rabin. Flory-type theory of a knotted ring polymer. *Phys Rev E*, 54:6618–6622, 1996.
- [6] VV Rybenkov, NR Cozzarelli, and AV Vologodskii. Probability of DNA knotting and the effective diameter of the DNA double helix. *Proc Nat Acad Sci*, 90:5307–5311, 1993.
- [7] SY Shaw and JC Wang. Knotting of a DNA chain during ring closure. *Science*, 260:533–536, 1993.
- [8] Y Diao, C Ernst, A Montemayor, EJ Rawdon, and U Ziegler. The knot spectrum of confined random equilateral polygons. *Comp Mathl Biophys*, 2(1), 2014.
- [9] C Ernst, EJ Rawdon, and Z Ziegler. Knotting spectrum of polygonal knots in extreme confinement. *J Phys A: Math Theor*, 54(23):235202, 2021.
- [10] Y Diao, C Ernst, A Montemayor, and U Ziegler. Generating equilateral random polygons in confinement. *J Phys A: Math Theor*, 44(40):405202, 2011.
- [11] Y Diao, C Ernst, A Montemayor, and U Ziegler. Generating equilateral random polygons in confinement II. *J Phys A: Math Theor*, 45(27):275203, 2012.
- [12] Y Diao, C Ernst, A Montemayor, and U Ziegler. Generating equilateral random polygons in confinement III. *J Phys A: Math Theor*, 45(46):465003, 2012.
- [13] Y Diao, C Ernst, EJ Rawdon, and U Ziegler. Total curvature and total torsion of knotted random polygons in confinement. *J Phys A: Math Theor*, 51(15):154002, 2018.
- [14] J Cantarella, H Schumacher, and C Shonkwiler. A faster direct sampling algorithm for equilateral closed polygons and the probability of knotting. *J Phys A: Math Theor*, 57(28):285205, 2024.
- [15] J Cantarella, H Chapman, and M Mastin. Knot probabilities in random diagrams. *J Phys A: Math Theor*, 49(40):405001, 2016.
- [16] SL Witte. *Link nomenclature, random grid diagrams, and Markov chain methods in knot theory*. PhD thesis, 2020.
- [17] E Orlandini, AL Stella, and C Vanderzande. Loose, flat knots in collapsed polymers. *J Stat Phys*, 115:681–700, 2004.

- [18] ME Cates and JM Deutsch. Conjectures on the statistics of ring polymers. *Journal de Physique*, 47(12):2121–2128, 1986.
- [19] J Arsuaga, M Vázquez, S Trigueros, DW Sumners, and J Roca. Knotting probability of DNA molecules confined in restricted volumes: DNA knotting in phage capsids. *Proc Nat Acad Sci*, 99(8):5373–5377, 2002.
- [20] F Slongo, Hauke P, Faccioli P, and Micheletti C. Quantum-inspired encoding enhances stochastic sampling of soft matter systems. *Sci Adv*, 9:eadi0204, 2023.
- [21] JPJ Michels and FW Wiegel. Probability of knots in a polymer ring. *Phys Lett A*, 90:381–384, 1982.
- [22] AV Vologodskii, SD Levene, KV Klenin, M Frank-Kamenetskii, and NR Cozzarelli. Conformational and thermodynamic properties of supercoiled dna. *J Mol Bio*, 227(4):1224–1243, 1992.
- [23] EJ Janse van Rensburg. The probability of knotting in lattice polygons. *Contemp Math*, 304:125–136, 2002.
- [24] EJ Janse van Rensburg and A Rechnitzer. Generalized atmospheric sampling of knotted polygons. *J Knot Theo Ram*, 20:1145–1171, 2011.
- [25] EJ Janse van Rensburg and SG Whittington. The BFACF algorithm and knotted polygons. *J Phys A: Math Gen*, 24:5553–5567, 1991.
- [26] EJ Janse van Rensburg. Squeezing knots. *J Stat Mech: Theo Expr*, 2007:P03001, 2007.
- [27] R Matthews, AA Louis, and JM Yeomans. Confinement of knotted polymers in a slit. *Mol Phys*, 109:1289–1295, 2011.
- [28] EJ Janse van Rensburg, E Orlandini, MC Tesi, and SG Whittington. Knotting in stretched polygons. *J Phys A: Math Theo*, 41:015003, 2008.
- [29] EJ Janse van Rensburg, E Orlandini, MC Tesi, and SG Whittington. Knot probability of polygons subjected to a force: a Monte Carlo study. *J Phys A: Math Theo*, 41:025003, 2008.
- [30] C Vanderzande. On knots in a model for the adsorption of ring polymers. *J Phys A: Math Gen*, 28:3681–3700, 1995.
- [31] MC Tesi, EJ Janse van Rensburg, E Orlandini, DW Sumners, and SG Whittington. Knotting and supercoiling in circular DNA: a model incorporating the effect of added salt. *Phys Rev E*, 49:868–872, 1994.
- [32] D Gasumova, EJ Janse van Rensburg, and A Rechnitzer. Lattice knots in a slab. *J Stat Mech:*

- Theo Expr*, 2012(09):P09004, 2012.
- [33] EJ Janse van Rensburg. The entropic pressure of lattice knots. *J Stat Mech: Theo Expr*, 2014(6):P06017, 2014.
- [34] EJ Janse van Rensburg. Osmotic pressure of compressed lattice knots. *Phys Rev E*, 100:012501, 2019.
- [35] J Tang, N Du, and PS Doyle. Compression and self-entanglement of single DNA molecules under uniform electric field. *Proc Nat Acad Sci*, 108(39):16153–16158, 2011.
- [36] CB Renner. *Studying self-entangled DNA at the single molecule level*. PhD thesis, Massachusetts Institute of Technology, 2015.
- [37] EJ Janse van Rensburg and A Rechnitzer. Generalized atmospheric sampling of self-avoiding walks. *J Phys A: Math Theo*, 42:335001, 2009.
- [38] A Rechnitzer and EJ Janse van Rensburg. Generalized atmospheric Rosenbluth methods (GARM). *J Phys A: Math Theo*, 41:442002, 2008.
- [39] EJ Janse van Rensburg. The free energy of compressed lattice knots. *J Phys A: Math Theo*, 53:015002, 2019.
- [40] EJ Janse van Rensburg and SD Promislow. Minimal knots in the cubic lattice. *J Knot Theo Ram*, 4:115–130, 1995.
- [41] EJ Janse van Rensburg and A Rechnitzer. Minimal knotted polygons in cubic lattices. *J Stat Mech: Theo Expr*, 2011(09):P09008, 2011.
- [42] Y Diao. Minimal knotted polygons on the cubic lattice. *J Knot Theo Ram*, 2:413–425, 1993.
- [43] R Scharein, K Ishihara, J Arsuaga, Y Diao, K Shimokawa, and M Vazquez. Bounds for the minimum step number of knots in the simple cubic lattice. *J Phys A: Math Theor*, 42(47):475006, 2009.
- [44] DW Sumners and SG Whittington. Knots in self-avoiding walks. *J Phys A: Math Gen*, 21:1689–1694, 1988.
- [45] EJ Janse van Rensburg. Minimal lattice knots. In A Stasiak, V Katritch, and LH Kaugman, editors, *Ideal Knots*, volume 19 of *Series on Knots and Everything*, pages 88–106. World Scientific, Singapore, 1999.
- [46] EJ Janse van Rensburg. Thoughts on lattice knot statistics. *J Math Chem*, 45:7–38, 2009.
- [47] R Guida and J Zinn-Justin. Critical exponents of the n -vector model. *J Phys A: Math Gen*, 31:8103–8122, 1998.

- [48] JC Le Guillou and J Zinn-Justin. Accurate critical exponents from field theory. *J de Phys*, 50:1365–1370, 1989.
- [49] E Orlandini, MC Tesi, EJ Janse van Rensburg, and SG Whittington. Entropic exponents of lattice polygons with specified knot type. *J Phys A: Math Gen*, 29:L299–L304, 1996.
- [50] B Berg and D Foerster. Random paths and random surfaces on a digital computer. *Phys Lett B*, 106:323–326, 1981.
- [51] C Aragao de Carvalho, S Caracciolo, and J Fröhlich. Polymers and $g\phi^4$ -theory in four dimensions. *Nucl Phys B*, 215:209–248, 1983.
- [52] EJ Janse van Rensburg and A Rechnitzer. Atmospheres of polygons and knotted polygons. *J Phys A: Math Theo*, 41:105002, 2008.
- [53] EJ Janse van Rensburg and A Rechnitzer. The compressibility of minimal lattice knots. *J Stat Mech: Theo Expr*, 2012:P05003, 2012.
- [54] EJ Janse van Rensburg and SG Whittington. The knot probability in lattice polygons. *J Phys A: Math Gen*, 23:3573–3590, 1990.
- [55] PJ Flory. Thermodynamics of high polymer solutions. *J Chem Phys*, 10:51–61, 1942.
- [56] PJ Flory. *Principles of Polymer Chemistry*. Cornell University Press, London, 1953.
- [57] ML Huggins. Some properties of solutions of long-chain compounds. *J Phys Chem*, 46:151–158, 1942.
- [58] MA Anisimov, TJ Longo, and JV Sengers. Critical fluctuations in polymer solutions: Crossover from criticality to tricriticality. In *50 Years of the Renormalization Group: Dedicated to the Memory of Michael E Fisher*, pages 119–145. World Scientific, 2024.
- [59] EJ Janse van Rensburg, E Orlandini, MC Tesi, and SG Whittington. Thermodynamic and topological properties of copolymer rings with a segregation/mixing transition. *J Phys A: Math Theo*, 55(43):435002, 2022.
- [60] EJ Janse van Rensburg, SG Whittington, and N Madras. The pivot algorithm and polygons: results on the FCC lattice. *J Phys A: Math Gen*, 23(9):1589–1612, May 1990.
- [61] EJ Janse van Rensburg. *Monte Carlo methods for lattice polygons*, pages 203–233. Springer Netherlands, Dordrecht, 2009.
- [62] S Campbell and EJ Janse van Rensburg. Parallel PERM. *J Phys A: Math Theo*, 53(26):265005, 2020.
- [63] EJ Janse van Rensburg and SG Whittington. The dimensions of knotted polygons. *J Phys*

A: *Math Gen*, 24(16):3935, 1991.